



Magnetic nanoparticles tris(hydrogensulfato) boron as an efficient heterogeneous acid catalyst for the synthesis of α,α -benzylidene bis(4-hydroxycoumarin) derivatives under solvent-free condition

Payam Hayati¹ · Khadijeh Eghbali² · Ramin Rezaei²

Received: 5 March 2019 / Accepted: 5 June 2019
© Springer Nature B.V. 2019

Abstract

Nano-ferrite supported tris(hydrogensulfato) boron $[\text{Fe}_3\text{O}_4@\text{B}(\text{HSO}_4)_3]$ was prepared by entrapping Fe_3O_4 magnetic nanoparticles as the core and tris(hydrogensulfato) boron $\text{B}(\text{HSO}_4)_3$ as the outer shell. This effective and magnetically recoverable catalyst was employed for the synthesis of α,α -benzylidene bis(4-hydroxycoumarin) derivatives through the reaction of an aromatic aldehyde and 4-hydroxycoumarin under solvent-free conditions. This acid catalyst was characterized by Fourier transform infrared spectroscopy, X-ray diffraction analysis, scanning electron microscopy, transmission electron microscopy, thermal gravimetric analysis and differential scanning calorimetry, energy-dispersive X-ray spectroscopy, Brunauer–Emmett–Teller analysis, Barret–Joyner–Halenda analysis, vibrating sample magnetometer and titration.

Keywords Magnetic nanoparticles · Multicomponent reactions · Heterogeneous catalysts · Biscoumarins · Tris (hydrogensulfato) boron

Introduction

One of the most common practical methods in the chemical industry is a request for acid catalysts [1]. Homogeneous catalysts have several disadvantages over heterogeneous alternatives, such as equipment corrosion, manufacturing of waste, trouble in separation and recycling, high charge and reduced effectiveness [2]. Polymers [3],

✉ Ramin Rezaei
rezaieramin@yahoo.com

¹ Persian Gulf Science and Technology Park, Nano Gostaran Navabegh Fardaye Dashtestan Company, Borazjan, Iran

² Department of Chemistry, Firoozabad Branch, Islamic Azad University, Firoozabad, Iran

mesoporous components [4], metal oxides [5] and nanoparticles [6] are generally applied as support for the more simplistic heterogeneous catalytic synthesis.

Magnetite Fe_3O_4 nanoparticles have now attracted wide consideration in the field of biology, medicine, electronics, and catalytic processes [7]. The high surface concentrations of hydroxyl groups on the Fe_3O_4 nanoparticles have led to large increases in hydrophilic nature of these nanoparticles [8, 9]. The excellent capacity and stability of the core/shell nanostructure (CSNs) could be related to both the core and the shell framework. This composite system includes the benefits of both the core and the shell leading to improvement of physical and chemical properties. A few synthetic methods for providing various classes of CSNs, including the Stöber technique, solvothermal method and one-pot synthetic method concerning surfactants have already been described [10]. There were numerous efforts to stabilize Fe_3O_4 nanoparticles whose surfaces have been coated with organic and inorganic compounds. Magnetic nanoparticles that could be magnetized in the current presence of an external magnet have been properly used as catalysts in a number of different organic and inorganic reactions due to the high surface-to-volume ratio of nanomaterial and imply that the large ratio of atoms is offered at the surface. In addition, the first and most important advantages of these catalysts based on the kind of reaction are revealed to be effective, the other is to maintain their catalytic activity. Therefore, these magnetic catalysts are efficiently applied as catalytic systems in lots of chemical reactions [11–16].

Boric acid is commonly used for the production of monofilament fiberglass [17], fire retarding agent of wood by impregnation [18], neutralizing active hydrofluoric acid (HF) [19], combined with borax [20] and silicone oil [21] for industrial applications.

Following Kiasat's report on the planning of tris(hydrogensulfato) boron [22], many advantages such as low price, non-toxicity and adaptation to the environment in particular are reported for this compound. The reason for these features is dual Lewis- Bronsted acidic sites. Because of these properties, attention has been significantly focused on catalytic applications of tris(hydrogensulfato) boron in catalyzing some organic reactions [23–28]. Additionally, silica boron-sulfuric acid nanoparticles have been organized as a heterogeneous catalyst in the Ritter reaction and the synthesis of amide derivatives [29]. Synthesis of nano- Fe_3O_4 @ SiO_2 -supported boron sulfonic acid and its application as heterogeneous catalyst for the synthesis of pyrano coumarins was reported by Farahi et al. [30].

During previous decades, the synthesis of coumarin derivatives was an essential field for investigation of biological properties such as anti-HIV, antibiotic, antifungal, antibacterial, antioxidant, anticancer and anticoagulants [31–33]. Furthermore, these compounds found a number of applications such as fluorescent brighteners, effective laser dyes, and as additives in food and cosmetics [34–36]. Amongst numerous well-known derivatives of coumarin, biscoumarins are significantly of more interest. Pechmann, Perkin, Knoevenagel, Reformatsky, and Wittig reactions are the most important synthetic methods for preparation of biscoumarins. The generally applied method which has been used for preparation of biscoumarin derivatives is the Knoevenagel reaction of two equivalents of 4-hydroxycoumarin and various aldehydes in the presence of different catalysts like molecular iodine [37],

[bmim][BF₄] [38], TBAB [39], SDS [40], sulfated titania [41], SO₃H functionalized ionic liquids [42], [P₄VPy BuSO₃H]HSO₄ [43], silica-supported preyssler nanoparticles [44], magnetite-containing sulfonated polyacrylamide [45], CuO–CeO₂ nanocomposite [46], Montmorillonite K10·Ni⁰·Mont [47], B(OSO₃H)₃ [25], etc.

According to previous research [48, 49], a novel, active, recyclable, and magnetically recoverable heterogeneous catalyst is reported in this paper. The aims of this research include obtaining the smallest particle size, reduction in the number of catalyst preparation steps and morphological control for increasing reaction which makes the obtained results to be comparable with other reported methods [29, 30]. Additionally, the preparation of magnetic tris (hydrogensulfato) boron [Fe₃O₄@B(HSO₄)₃] that has been used as an effective catalyst for the synthesis of biscoumarin derivatives is also reported in this paper

Experimental

Materials and methods

Laboratory chemicals were either prepared in our laboratory or were purchased from Merck and Fluka. Melting points were determined in open capillaries with IA 9100 Series Digital Melting Point apparatus. IR spectra were obtained at 4000–400 cm⁻¹ with KBr pressed powder discs using a 4300 Shimadzu FT-IR spectrometer. ¹H and ¹³C NMR spectra were recorded in CDCl₃ as solvent using a Bruker Avance 400 MHz spectrometer. The crystal structure of the resulting powder was examined by powder X-ray diffraction (XRD; Bruker D8 Advance TXS) using Cu K α radiation. Scanning electron microscopy (SEM) was performed on a MIRA III SEM, Czech Republic, operated at a 15 kV accelerating voltage. We performed a transmission-electron-microscopy (TEM) study on a JEOL, JEM-2100F transmission electron microscope at an accelerating voltage of 200 kV. The Barret–Joyner–Halender (BJH) specific surface areas were measured by nitrogen adsorption–desorption at –77 K using a Belsorp mini II apparatus. The BJH method was used to determine the pore size distribution. The thermal properties of Fe₃O₄, B(HSO₄)₃ and Fe₃O₄@B(HSO₄)₃ were further evaluated with TGA and DSC using a TG thermoanalyser (TGA, Mettler system TA 4000) in N₂ at a heating rate of 10 °C min⁻¹. EDX spectra were measured with a Bruker XFlash 6130 for analyzing phase composition and elemental distribution maps of the compounds.

Preparation of magnetic Fe₃O₄ nanoparticles

Coprecipitation technique with small changes was used for preparation of magnetic Fe₃O₄ nanoparticles. First, FeCl₂·4H₂O (2.00 g, 10.0 mmol) and FeCl₃·6H₂O (5.40 g, 20.0 mmol) were dissolved in 2 M hydrochloric acid solutions (25.0 mL). Then under mechanical stirring, ammonia solution (30.0 mL, 25.0%) was added to the FeCl₂/FeCl₃ mixture. After ~30 min of intense stirring, the resulting black precipitate was easily isolated by a magnetic field and thoroughly washed with 2.0 M

hydrochloric acid and deionized water, respectively, and finally was ball milled for ~1 h at room temperature.

Preparation of tris(hydrogensulfato)boron $B(HSO_4)_3$

A 250 mL suction flask charged with boric acid (1.55 g, 25.0 mmol) was equipped with a gas inlet tube for conducting HCl gas over an adsorbing solution, i.e., water. Chlorosulfonic acid (8.74 g, ~5.0 mL, ~75.0 mmol) was added in small portions over a period of 30 min at 0 °C. HCl evolved from the reaction vessel immediately. After completion of the addition, the mixture was shaken for 1 h, while the residual HCl was eliminated by suction. Then the mixture was washed with diethyl ether to remove the unreacted chlorosulfonic acid, giving a grayish solid material in 90% yield (~6.8 g).

Preparation of $Fe_3O_4@B(HSO_4)_3$ nanoparticles

The 0.10 g (0.43 mmol) Fe_3O_4 NPs and 0.10 g PVP were dispersed in a mixture of methanol and deionized water, (10 mL 1:1), under continuous mechanical stirring, and $B(HSO_4)_3$ nanoparticles (0.40 g, 1.32 mmol) were added to the reaction mixture over a period of ~30 min at room temperature. The mixture was stirred at 80 °C for ~24 h. The separated powder was cooled down to room temperature, and was washed with deionized water and absolute ethanol and dried at 60 °C overnight. Afterward, it was calcinated in an oven furnace at 600 °C for 2 h with a heating rate of 4 °C min⁻¹.

Titration of $Fe_3O_4@B(HSO_4)_3$ nanoparticles

Dry $Fe_3O_4@B(HSO_4)_3$ (0.10 g) was added to distilled water (10.0 mL) and the resulting mixture was stirred for 24 h and then titrated with aqueous solution of NaOH (0.10 M) as titrant and phenolphthalein as an indicator. The acidic sites loading in $Fe_3O_4@B(HSO_4)_3$ was found to be 3.50 mmol/g.

General procedure for the preparation of biscoumarin derivatives

A mixture of 4-hydroxycoumarin (0.32 g, 2.0 mmol), aldehyde (1.0 mmol), $Fe_3O_4@B(HSO_4)_3$ (0.1 g, 0.03 mol %) were mixed completely and heated in an oil bath at 80 °C for the appropriate time as mentioned in Table 4. Following completion of the reaction as monitored by TLC, ethyl acetate (10.0 mL) was added to the mixture, and the catalyst was separated from the reaction medium by using a magnet (2×10^{-2} T). The organic layer was separated, concentrated, dried over anhydrous sodium sulfate and evaporated. A pure product was obtained through crystallization using ethanol as solvent. The biscoumarin derivatives are characterized by comparison of their physical and spectral data to those reported in the literature.

General procedure for recycling of $\text{Fe}_3\text{O}_4@\text{B}(\text{HSO}_4)_3$ nanoparticles

The catalytic recyclability of $\text{Fe}_3\text{O}_4@\text{B}(\text{HSO}_4)_3$ was done by adding ethanol (2×15 mL) to remove the organic compounds and dried in an oven at 80°C for 3 h. The results show that the catalyst is magnetically recoverable and this process was repeated four times without any significant loss of activity.

Spectral analysis of compounds (3a–i)

3,3'-(Phenylmethylene)-bis(4-hydroxy-2H-chromen-2-one) (3a) White crystals; mp: $222\text{--}224^\circ\text{C}$ (lit.: $228\text{--}230^\circ\text{C}$) [37].; FT-IR: ν (cm^{-1}) 3428, 3035, 1665, 1608, 764; ^1H NMR: δ (ppm) 6.50 (s, 1H, CH), 7.25–8.26 (m, 13H, ArH); 11.33 (s, 1H, OH), 11.60 (s, 1H, OH); ^{13}C NMR: δ (ppm) 37.14, 103.28, 106.64, 116.40, 116.75, 124.35, 124.93, 126.85, 128.70, 132.58, 136.22, 153.17, 164.50, 166.02; Anal. Calcd for $\text{C}_{25}\text{H}_{16}\text{O}_6$ (411.78): C, 72.81; H, 3.91. Found: C, 72.65; H, 3.83.

3,3'-(2-Hydroxyphenylmethylene)-bis(4-hydroxy-2H-chromen-2-one) (3b) Yellow crystals; mp: $240\text{--}242^\circ\text{C}$ (lit.: $254\text{--}256^\circ\text{C}$) [37].; FT-IR: ν (cm^{-1}) 3353, 3045, 1710, 1625, 760; ^1H NMR: δ (ppm) 6.43 (s, 1H, CH), 7.15–8.15 (m, 12H, ArH); 8.65 (s, 1H, OH), 11.60 (s, 1H, OH); ^{13}C NMR: δ (ppm) 34.3, 102.89, 116.75, 124.33, 125.15, 128.22, 129.55, 131.15, 133.28, 150.85; Anal. Calcd for $\text{C}_{25}\text{H}_{16}\text{O}_7$ (428.78): C, 70.09; H, 3.76. Found: C, 70.65; H, 3.85.

3,3'-(3-Nitrophenylmethylene)-bis(4-hydroxy-2H-chromen-2-one) (3c) Yellow crystals; mp: $126\text{--}128^\circ\text{C}$ (lit.: $120\text{--}124^\circ\text{C}$) [37].; FT-IR: ν (cm^{-1}) 3424, 2928, 1658, 1589, 1333, 765; ^1H NMR: δ (ppm) 6.15 (s, 1H, CH), 7.23–8.18 (m, 12H, ArH); 11.58 (s, 2H, OH), ^{13}C NMR: δ (ppm) 34.55, 102.88, 116.8, 124.77, 125.53, 127.9, 129.5, 131.9, 134.25, 149.86; Anal. Calcd for $\text{C}_{25}\text{H}_{15}\text{NO}_8$ (456.78): C, 65.65; H, 3.31; N, 3.06. Found: C, 65.70; H, 3.33, N, 3.15.

3,3'-(4-Methoxyphenylmethylene)-bis(4-hydroxy-2H-chromen-2-one) (3d) White crystals, mp: $240\text{--}242^\circ\text{C}$ (lit.: $247\text{--}249^\circ\text{C}$) [47].; FT-IR: ν (cm^{-1}): 3380, 3033, 1665, 1602, 1256, 1050, 767; ^1H NMR: δ (ppm) 3.70 (s, 3H, OCH_3), 6.48 (s, 1H, CH), 7.15–8.18 (m, 12H, ArH), 11.35 (s, 1H, OH), 11.50 (s, 1H, OH); ^{13}C NMR: δ (ppm) 32.12, 110.53, 116.3, 116.7, 120.92, 123.62, 124.1, 124.86, 128.12, 128.8, 134.52, 153.18, 156.52, 163.33, 165.21; Anal. Calcd for $\text{C}_{26}\text{H}_{18}\text{O}_7$ (443.56): C, 70.58; H, 4.10. Found: C, 70.78; H, 3.93.

3,3'-(4-Hydroxyphenylmethylene)-bis(4-hydroxy-2H-chromen-2-one) (3e) White crystals, mp: $218\text{--}220^\circ\text{C}$ (lit.: $222\text{--}225^\circ\text{C}$) [47].; FT-IR: ν (cm^{-1}): 3345, 3044, 1668, 1610, 760, ^1H NMR: δ (ppm) 6.46 (s, 1H, CH), 7.17–8.15 (m, 12H, ArH), 9.80 (s, 1H, OH), 11.35 (s, 1H, OH), 11.67 (s, 1H, OH); ^{13}C NMR: δ (ppm) 36.40, 103.15, 115.50, 116.85, 123.10, 126.59, 127.75, 151.85, 154.39, 164.52; Anal. Calcd for $\text{C}_{25}\text{H}_{16}\text{O}_7$ (429.82): C, 70.09; H, 3.76. Found: C, 70.62; H, 4.06.

3,3'-(4-Nitrophenylmethylene)-bis(4-hydroxy-2H-chromen-2-one) (3f) Yellow crystals, mp: 238–240 °C (lit.: 232–234 °C) [47].; FT-IR: ν (cm⁻¹): 3452, 3037, 1650, 1615, 1346, 1085, 760; ¹H NMR: δ (ppm) 6.60 (s, 1H, CH), 7.43–8.35 (m, 12H, ArH); 11.45 (s, 1H, OH), 11.55 (s, 1H, OH); ¹³C NMR: δ (ppm) 35.2, 103.52, 105.12, 116.86, 117.13, 121.16, 122.15, 124.63, 125.87, 130.15, 132.5, 134.38, 137.44, 147.72, 151.2, 163.54, 166.32, 166.9; Anal. Calcd for C₂₅H₁₅NO₈ (458.43): C, 65.65; H, 3.31; N, 3.06. Found: C, 65.77; H, 3.30; N, 2.88.

3,3'-(4-Chlorophenylmethylene)-bis(4-hydroxy-2H-chromen-2-one) (3g) White crystals, mp: 246–248 °C (lit.: 255–257 °C) [47].; FT-IR: ν (cm⁻¹): 3422, 3035, 2710, 1678, 1610, 1555, 1474, 1354, 1097, 765; ¹H NMR: δ (ppm) 6.40 (s, 1H, CH), 7.35–8.44 (m, 12H, ArH); 11.35 (s, 1H, OH), 11.50 (s, 1H, OH); ¹³C NMR: δ (ppm) 34.8, 104.39, 106.28, 117.5, 124.33, 125.18, 127.0, 128.82, 133.52, 134.12, 134.8, 153.44, 164.73, 165.9; Anal. Calcd for C₂₅H₁₅ClO₆ (445.68): C, 67.20; H, 3.38. Found: C, 67.10; H, 3.30.

3,3'-(3-phenylprop-2-ene-1,1-diyl)bis(4-hydroxy-2H-chromen-2-one) (3h) Yellow crystals, mp: 235–237 °C (lit.: 230–232 °C) [37].; FT-IR: ν (cm⁻¹): 3320, 3025, 1728, 1670, 1616, 760; ¹H NMR: δ (ppm) 6.55 (s, 1H, CH), 6.68 (d, J = 15.1 Hz, 1H, CH=), 6.75 (d, J = 15.1 Hz, 1H, CH=), 7.10–8.15 (m, 12H, ArH); 11.40 (s, 1H, OH), 11.55 (s, 1H, OH); ¹³C NMR: δ (ppm) 19.52, 94.17, 118.33, 123.85, 125.39, 126.2, 128.0, 128.51, 129.0, 129.47, 131.76, 138.24, 154.39, 164.48, 165.83; Anal. Calcd for C₂₇H₁₈O₆ (437.55): C, 73.97; H, 4.14. Found: C, 73.88; H, 4.05.

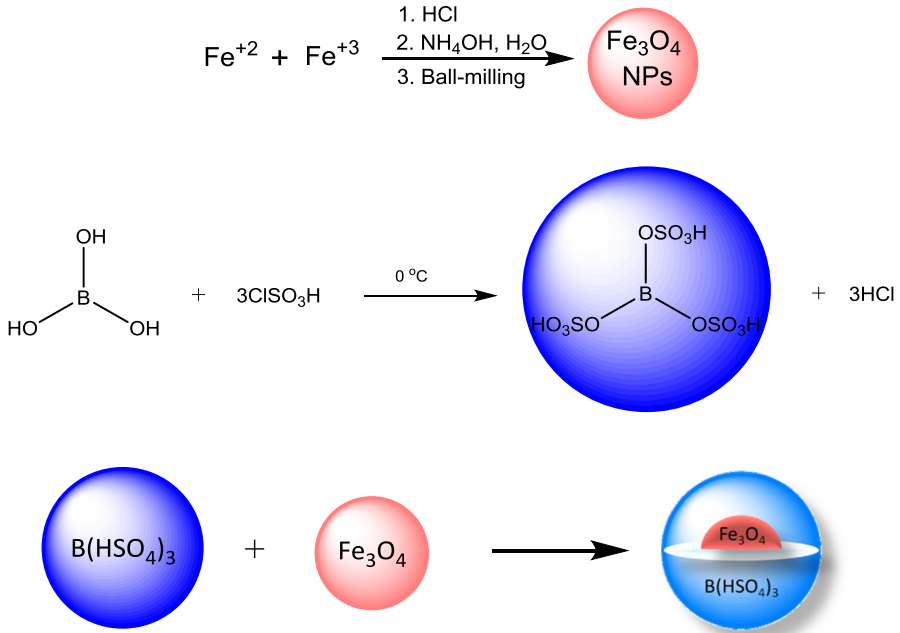
3,3'-(furan-2-ylmethylene)bis(4-hydroxy-2H-chromen-2-one) (3i) Black amorphous solid, mp: 194–196 °C (lit.: 202 °C) [37].; FT-IR: ν (cm⁻¹): 3033, 1656, 1608, 1330, 765; ¹H NMR: δ (ppm) 6.0 (s, 1H, CH), 6.30–6.59 (m, 3H, ArH), 7.32–8.35 (m, 8H, ArH); ¹³C NMR: δ (ppm) 22.16, 102.57, 107.28, 112.41, 116.8, 124.95, 125.46, 126.9, 128.81, 144.61, 153.19, 153.73, 163.38, 165.57; Anal. Calcd for C₂₃H₁₄O₇ (402.42): C, 68.66; H, 3.51. Found: C, 68.44; H, 3.46.

Results and Discussion

The magnetite nanoparticles were first synthesized by the co-precipitation of Fe²⁺ and Fe³⁺ in ammonia solution according to reported procedure [50]. Tris(hydrogensulfato)boron was prepared by addition of chlorosulfonic acid to boric acid [22]. Finally, magnetic-nanoparticle-supported tris(hydrogensulfato)boron was synthesized from the reaction of Fe₃O₄ with tris(hydrogensulfato)boron (Scheme 1).

Characterization of Fe₃O₄@B(HSO₄)₃

Measurement of the acidic sites of Fe₃O₄@B(HSO₄)₃ was determined by the titration method. Based on comparison of titration curves of B(HSO₄)₃ and



Scheme 1 Schematic representation of $\text{Fe}_3\text{O}_4@\text{B}(\text{HSO}_4)_3$ based on core/shell nanostructure

$\text{Fe}_3\text{O}_4@\text{B}(\text{HSO}_4)_3$ it was found that both curves have the same pattern and this reflects that $\text{B}(\text{HSO}_4)_3$ is part of the catalyst structure (Figs. 1, 2).

The results of FT-IR spectra of Fe_3O_4 , $\text{B}(\text{HSO}_4)_3$, and $\text{Fe}_3\text{O}_4@\text{B}(\text{HSO}_4)_3$ demonstrate the presence of different chemical bonds and functional groups in the structure of the $\text{Fe}_3\text{O}_4@\text{B}(\text{HSO}_4)_3$ compound (Fig. 3). The IR spectral data of Fe_3O_4 display

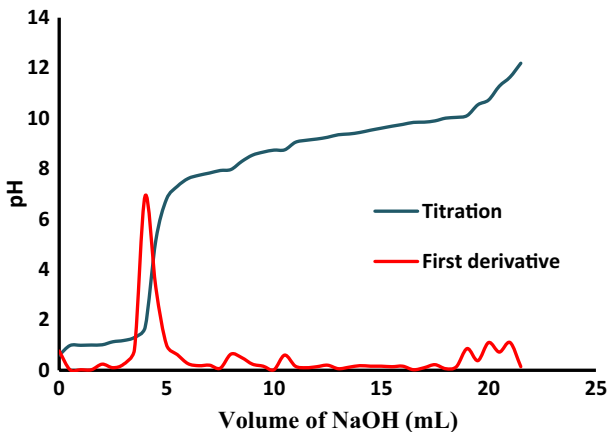


Fig. 1 Titration and its first derivative curves of the $\text{B}(\text{HSO}_4)_3$ with NaOH

Fig. 2 Titration and its first derivative curves of the $\text{Fe}_3\text{O}_4@\text{B}(\text{HSO}_4)_3$ with NaOH

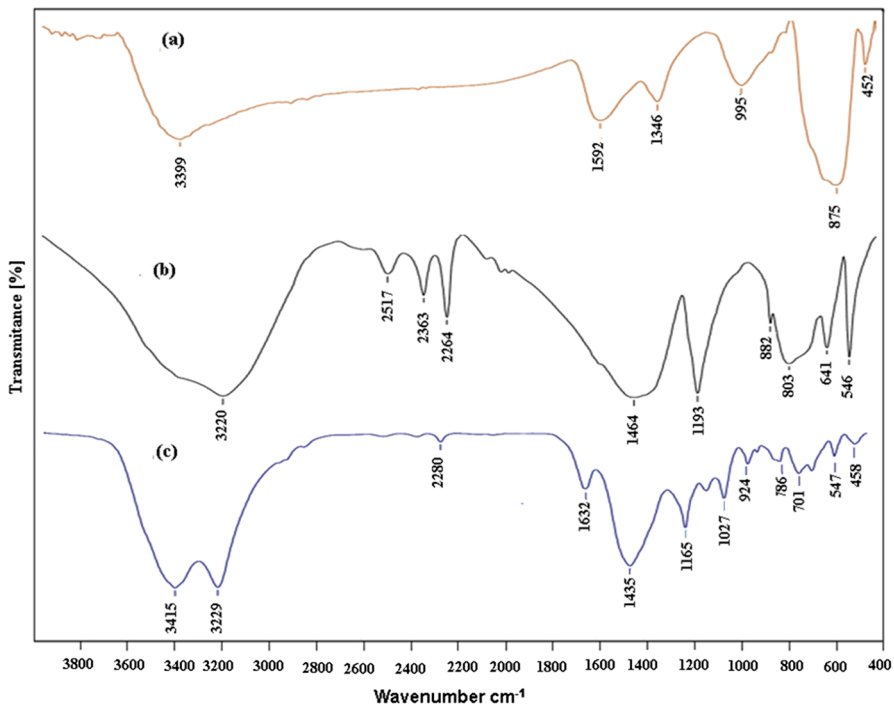
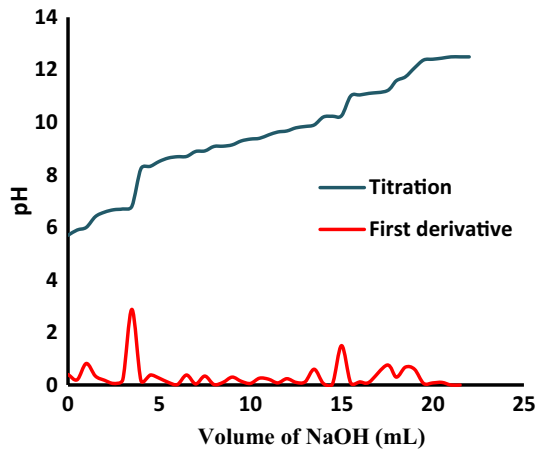


Fig. 3 FT-IR spectra of **a** Fe_3O_4 , **b** $\text{B}(\text{HSO}_4)_3$ and **c** $\text{Fe}_3\text{O}_4@\text{B}(\text{HSO}_4)_3$

two characteristic peaks at ~ 452 and ~ 875 cm^{-1} , which are a result of Fe–O stretching vibrations (Fig. 3a) [51]. The peak located at ~ 1464 cm^{-1} is in agreement with B–O bands (Fig. 3b) [51]. Furthermore, the symmetric stretching of the O=S=O fragment has been observed at ~ 1193 cm^{-1} (Fig. 3b) [52]. Also, in the IR spectrum of $\text{Fe}_3\text{O}_4@\text{B}(\text{HSO}_4)_3$ the appearance of peaks at 458 and 547, related to Fe–O

stretching vibrations, and shows that Fe_3O_4 nanoparticles were bonded to $\text{B}(\text{HSO}_4)_3$. Eventually, the appearance of peaks at 1165, and 1632 cm^{-1} can be attributed to B–O and symmetric stretching of the O=S=O, respectively. The appearance of peaks around 3229 and 3415 cm^{-1} can be assigned to the sulfonic group of the catalytic surface (Fig. 3c) [31].

The crystalline phases of Fe_3O_4 , $\text{B}(\text{HSO}_4)_3$ and $\text{Fe}_3\text{O}_4@ \text{B}(\text{HSO}_4)_3$ were investigated by XRD. All reflection peaks can be readily indexed to pure cell parameters $a=2.7992(3)\text{ \AA}$, $b=9.4097(15)\text{ \AA}$, and $c=9.4832(9)\text{ \AA}$ at 23.96 GPa and 823 K (ICDD: 190629). Fe^{3+} occupies an octahedral site and Fe^{2+} is in an eight-fold-coordinated site described as a bicapped trigonal prism. The XRD pattern of Fe_3O_4 nanoparticles (Fig. 4a) showed the peaks at $2\theta=17.70^\circ$, 29.0° , 31.95° , 35.50° , 43.20° , 45.10° , 53.85° , 57.05° , 63.30° , and 75.30° that could be assigned to 110, 220, 311, 222, 400, 110, 422, 511, 440, and 620 planes of Fe_3O_4 , respectively [53–55]. It can be seen in Fig. 4b that $\text{B}(\text{HSO}_4)_3$ presented the very strong diffraction peak at $2\theta=27.95$. The characteristic diffraction peak of $\text{B}(\text{HSO}_4)_3$ is associated with $\text{B}(\text{OH})_3$ with the pdf code (01-073-2158) [56]. The diffraction lines of $\text{Fe}_3\text{O}_4@ \text{B}(\text{HSO}_4)_3$ (Fig. 4c) correspond to the Fe_3O_4 nanoparticles based on the characteristic 2θ peaks at about 30.5, 34.50, 43.35, 57.60, and 61.50. Additionally, there was a peak at $2\theta=27.7$ due to the $\text{B}(\text{HSO}_4)_3$ shells of the coated Fe_3O_4 .

The SEM images of Fe_3O_4 , $\text{B}(\text{HSO}_4)_3$, and $\text{Fe}_3\text{O}_4@ \text{B}(\text{HSO}_4)_3$ NPs showed that the samples have spherical-like particles. There is a tendency to form small groups of particles due to weak forces (hydrogen bonding) between the $\text{Fe}_3\text{O}_4@ \text{B}(\text{HSO}_4)_3$ NPs (Fig. 5) [57]. This leads to a clustering tendency and produces a monodispersed structure of these magnetic nanoparticles.

Additionally the results of TEM imaging confirmed this observation (Fig. 6a). Based on Fig. 6b the average diameter identified from TEM images is 36 nm. It also shows that the maximum particle size distribution was in the range of 30–48 nm.

In order to show the thermodynamic behavior of the Fe_3O_4 , $\text{B}(\text{HSO}_4)_3$ and $\text{Fe}_3\text{O}_4@ \text{B}(\text{HSO}_4)_3$, TGA and DSC have been done (Fig. 7). The uncoated Fe_3O_4 NPs exhibits a rapid weight loss about 4% from ~ 50 to $\sim 300\text{ }^\circ\text{C}$ due to elimination of adsorbed physical and chemical water. Another weight loss was seen around $800\text{ }^\circ\text{C}$ which corresponds to decomposition of residual chemical compounds (Fig. 7a). TGA analysis of $\text{B}(\text{HSO}_4)_3$ demonstrated 40.0% weight loss between ~ 50 and $\sim 200\text{ }^\circ\text{C}$ is due to the dehydration of $\text{B}(\text{HSO}_4)_3$ that is similar to boric acid (H_3BO_3) [58]. In addition, a decrease in the weight percentage of $\text{B}(\text{HSO}_4)_3$ at temperatures up to $\sim 875\text{ }^\circ\text{C}$ is associated with the decomposition of sulfuric acid and oxidation of boron atoms (Fig. 7b). TGA and DSC of the $\text{Fe}_3\text{O}_4@ \text{B}(\text{HSO}_4)_3$ is shown in Fig. 7c. The first stage of weight loss between ~ 25 and $\sim 100\text{ }^\circ\text{C}$ is related to removal of physically adsorbed water. There is another weight loss between ~ 180 and $\sim 400\text{ }^\circ\text{C}$ that could be attributed to the thermal crystal phase transformations of Fe_3O_4 to Fe_2O_3 [45]. Based on thermal performance of the catalyst, decreases in the weight percentage of the catalyst at temperatures up to $\sim 650\text{ }^\circ\text{C}$ is related to decomposition of sulfuric acid and oxidation of boron atoms [29].

The elemental composition of Fe_3O_4 , $\text{B}(\text{HSO}_4)_3$ and $\text{Fe}_3\text{O}_4@ \text{B}(\text{HSO}_4)_3$ was obtained by using EDX analysis and the presence of Fe, O, B and S were confirmed by comparing between EDX spectra of that uncoated with Fe_3O_4 , $\text{B}(\text{HSO}_4)_3$ and

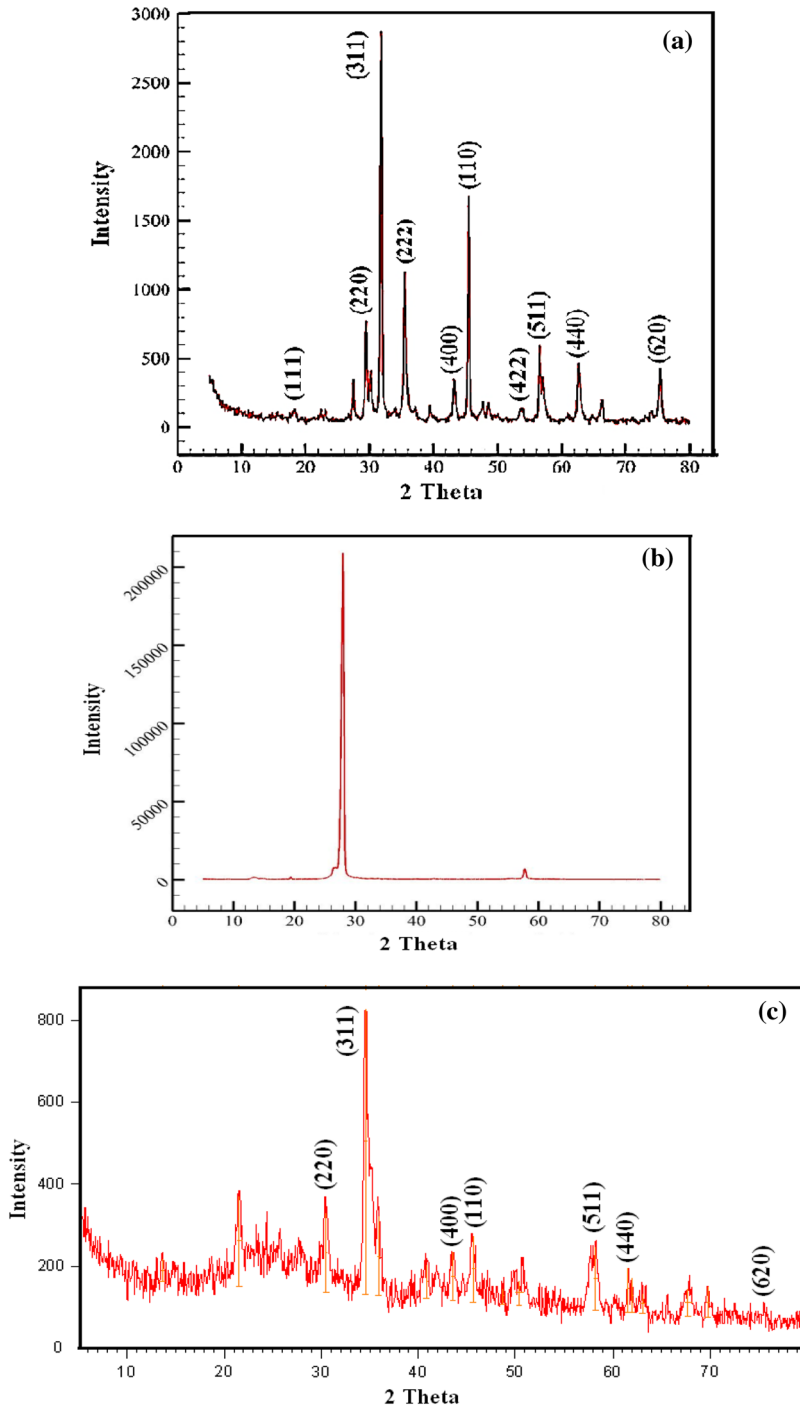


Fig. 4 Powder XRD pattern of **a** Fe_3O_4 , **b** $\text{B}(\text{HSO}_4)_3$ and **c** $\text{nano-Fe}_3\text{O}_4@ \text{B}(\text{HSO}_4)_3$

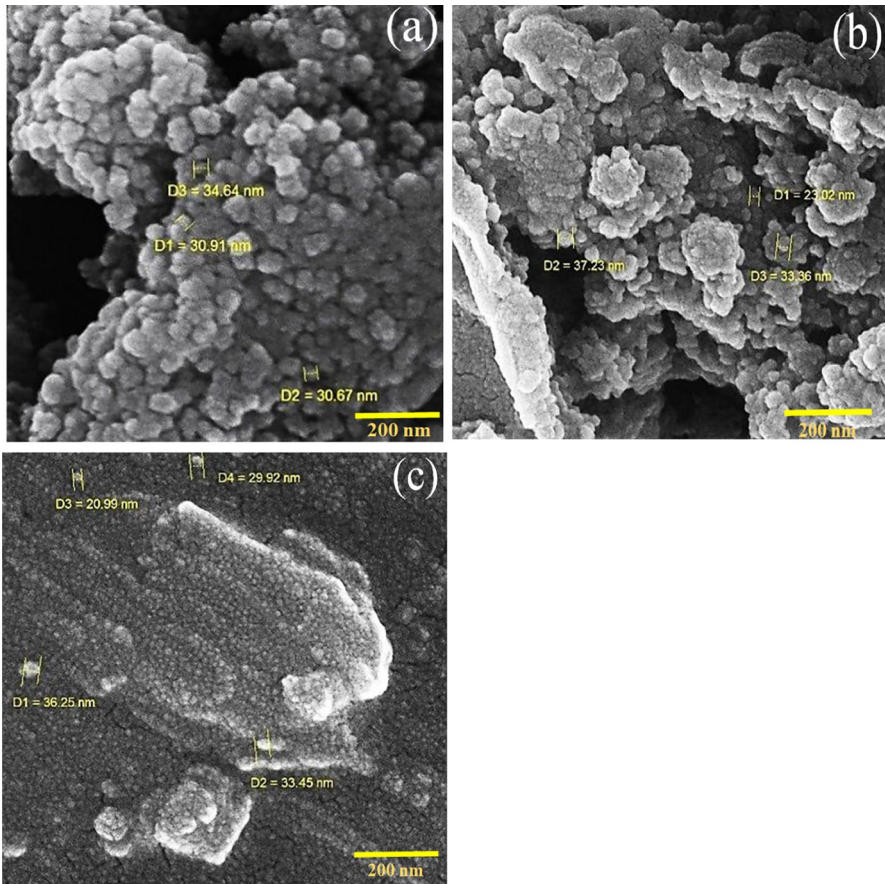


Fig. 5 SEM photographs of **a** Fe_3O_4 , **b** $\text{B}(\text{HSO}_4)_3$, and **c** $\text{Fe}_3\text{O}_4@\text{B}(\text{HSO}_4)_3$

$\text{Fe}_3\text{O}_4@\text{B}(\text{HSO}_4)_3$, although there were low amounts of sodium (a peak around 1 keV) and chlorine impurities (Fig. 8a, c), but the EDX analysis after four runs showed that these impurities have been eliminated (Fig. 13). It should be noted that the failure to detect the boron peak in Fig. 8c is due to the overlap between peaks of boron and other elements [30].

In addition, elemental mapping has been done on $\text{Fe}_3\text{O}_4@\text{B}(\text{HSO}_4)_3$ to obtain the exact information about distribution of Fe, O, S and B elements. Results and observations regarding patterns by the elemental mappings shows the uniform distribution of Fe, O, S, B and proves the homogeneity of $\text{B}(\text{HSO}_4)_3$ on the Fe_3O_4 (Fig. 9).

Based on the N_2 adsorption/desorption isotherm of $\text{Fe}_3\text{O}_4@\text{B}(\text{HSO}_4)_3$, it is clear that this isotherm could be classified as a type-IV of classical isotherms and displays a hysteresis loop at large relative pressures in the range of 0.64–0.98 P/Po [59], which is belonging to the H3 type [60]. $\text{Fe}_3\text{O}_4@\text{B}(\text{HSO}_4)_3$ nanostructures show a sharp peak at 9.23 nm indicating mesoporous characteristics (Fig. 10).

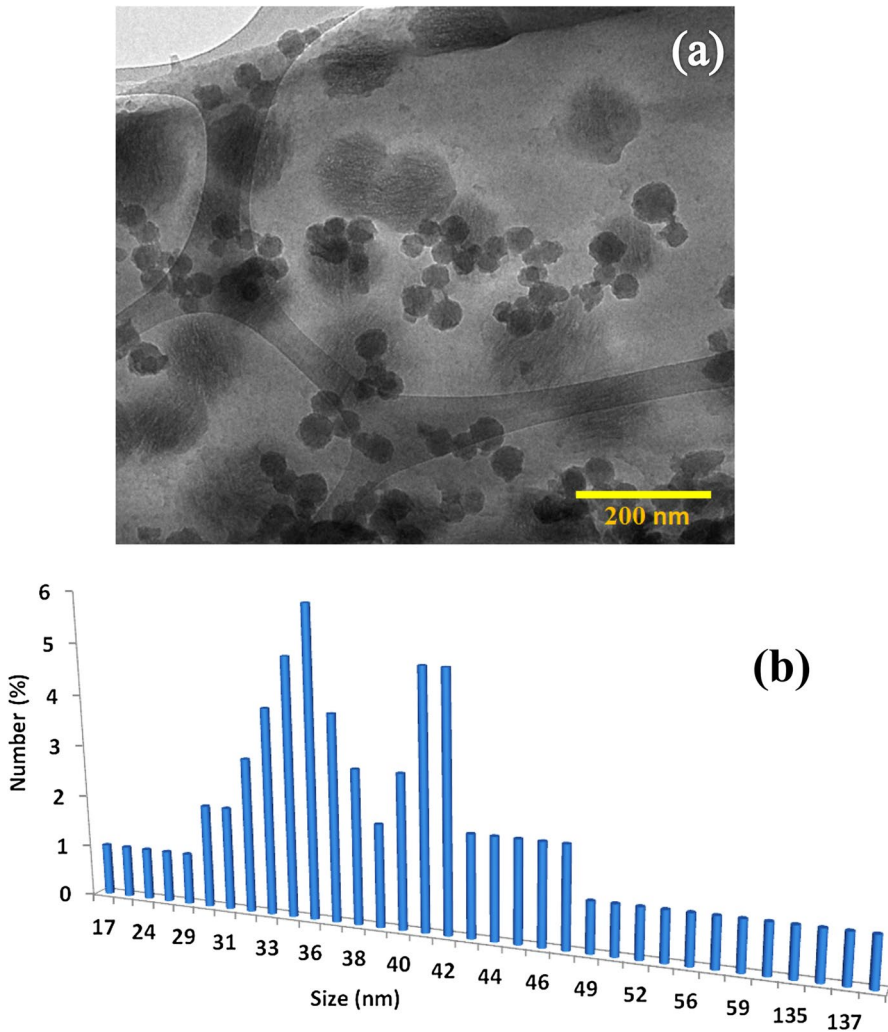


Fig. 6 TEM image of **a** $\text{Fe}_3\text{O}_4@\text{B}(\text{HSO}_4)_3$, and **b** size distributions of $\text{Fe}_3\text{O}_4@\text{B}(\text{HSO}_4)_3$

By using BET and BJH methods, surface area, pore volume, and pore size of $\text{Fe}_3\text{O}_4@\text{B}(\text{HSO}_4)_3$ were obtained and reported in Table 1.

To study the role of the $\text{B}(\text{HSO}_4)_3$ shell on the magnetic properties of this compound, measurements were carried out in a vibrating sample magnetometer (VSM) (Fig. 11). The saturation magnetization of the $\text{Fe}_3\text{O}_4@\text{B}(\text{HSO}_4)_3$ (~ 0.47 emu/g) (Fig. 11b) was less than Fe_3O_4 nanoparticles (~ 29.42 emu/g) (Fig. 11a) because there is interaction between $\text{B}(\text{HSO}_4)_3$ and Fe_3O_4 nanoparticles. This fact reveals a small coactivity with narrow hysteresis due to the soft magnetic properties for this nanostructure. These results are coming from the small particle size of Fe_3O_4 nanoparticles and cause an inverse correlation between coercivity and particle size [61].

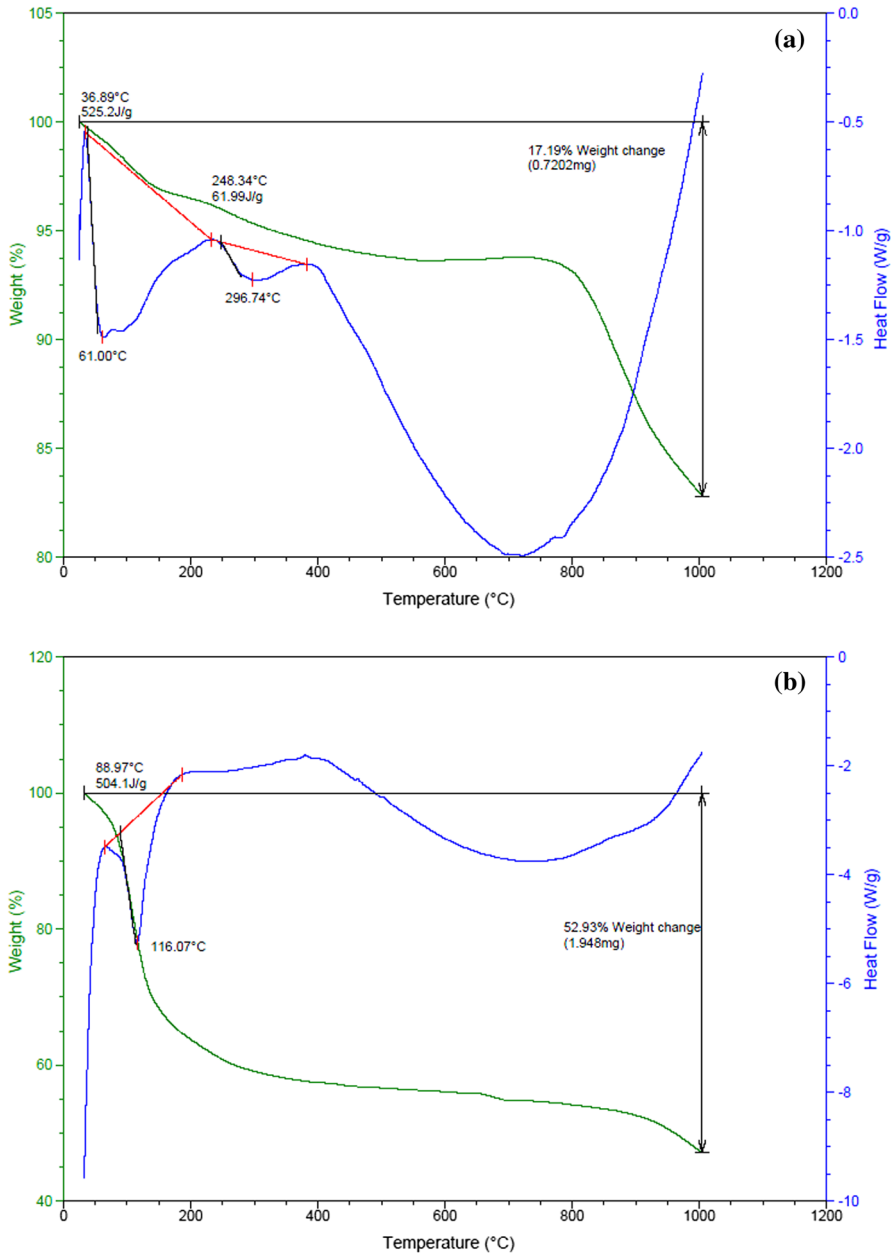


Fig. 7 TGA and DSC curves of **a** Fe₃O₄, **b** B(HSO₄)₃ and **c** Fe₃O₄@B(HSO₄)₃

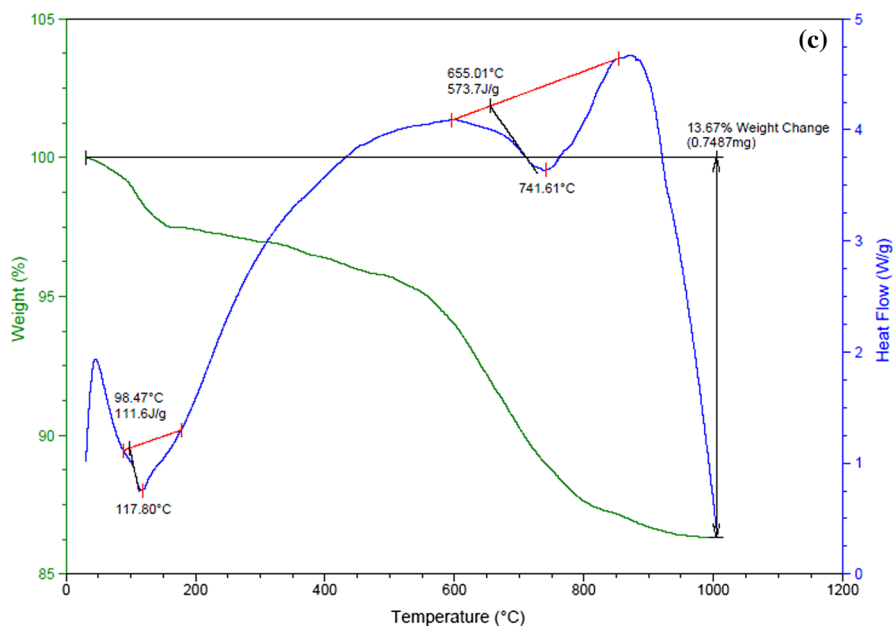


Fig. 7 (continued)

These observations confirm that the tris(hydrogensulfato) boron groups have functionalized the surface of the magnetite nanoparticles.

Catalytic performance of $\text{Fe}_3\text{O}_4@\text{B}(\text{HSO}_4)_3$ in multicomponent one-pot synthesis of dihydropyrimidinones

After synthesis of $\text{Fe}_3\text{O}_4@\text{B}(\text{HSO}_4)_3$, we investigate catalytic application of $\text{Fe}_3\text{O}_4@\text{B}(\text{HSO}_4)_3$ as a magnetically heterogeneous nanocatalysts for the synthesis of α,α -benzylidene bis(4-hydroxycoumarin) by carrying out the reaction with a 1:2 mol ratio of aldehyde and 4-hydroxycoumarin (Scheme 2).

In order to develop the reaction conditions and evaluation of catalytic performance of $\text{Fe}_3\text{O}_4@\text{B}(\text{HSO}_4)_3$, optimization reports could be carried out using the reaction of benzaldehyde and 4-hydroxycoumarin as a reaction model and the reaction conditions, including the amount of the catalyst, solvent, and reaction temperature result in quantifying the temperature and reaction time effects. Highlighting the usefulness and efficiency of $\text{Fe}_3\text{O}_4@\text{B}(\text{HSO}_4)_3$ it was examined in the absence of catalyst. It was found that in the absence of $\text{Fe}_3\text{O}_4@\text{B}(\text{HSO}_4)_3$ only 15% yield of the product was obtained even after heating at 80 °C for 120 min (Table 2, entry 1). Optimization of the amount of catalyst was achieved by varying the amount of catalyst (0.01, 0.03, and 0.05 wt%). The percentage of the product formation using $\text{Fe}_3\text{O}_4@\text{B}(\text{HSO}_4)_3$ as the catalyst was found 55, 90 and 90%, respectively (Table 2, entries 2–4). It should be added that the reaction did not proceed at room

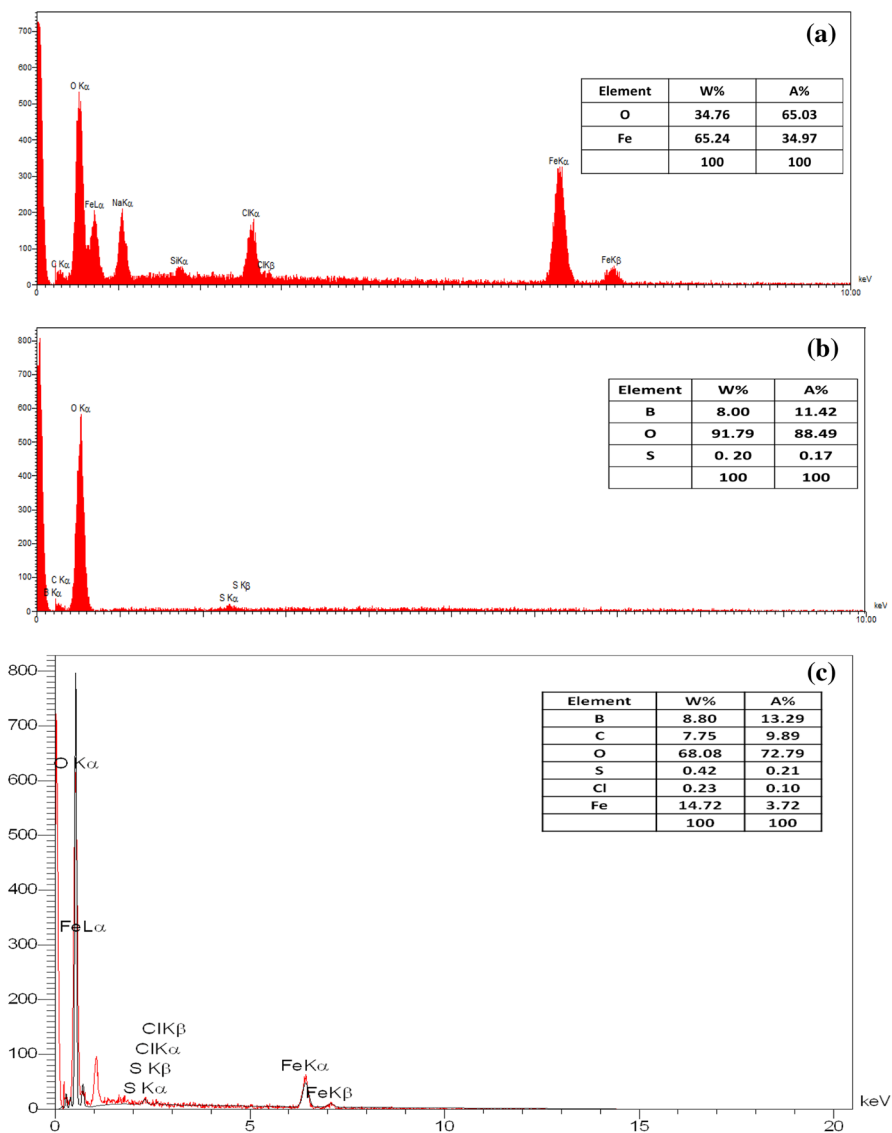


Fig. 8 EDX spectrum of **a** Fe_3O_4 , **b** $\text{B}(\text{HSO}_4)_3$ and **c** $\text{Fe}_3\text{O}_4@\text{B}(\text{HSO}_4)_3$

temperature (Table 2, entry 5). The reaction temperature was also optimized. Below 80 °C, the reaction proceeded slowly giving a relatively low yield and no significant improvement was observed above 80 °C (Table 2, entries 6–7). In order to investigate the effect of solvent on the catalytic reaction, the reaction model in the presence of 0.03 wt% $\text{Fe}_3\text{O}_4@\text{B}(\text{HSO}_4)_3$ was carried out in various solvents under reflux conditions. The results show that in the presence of solvents, the reaction was sluggish and H_2O is the best solvent in terms of both time and yield (Table 2, entries 8–11).

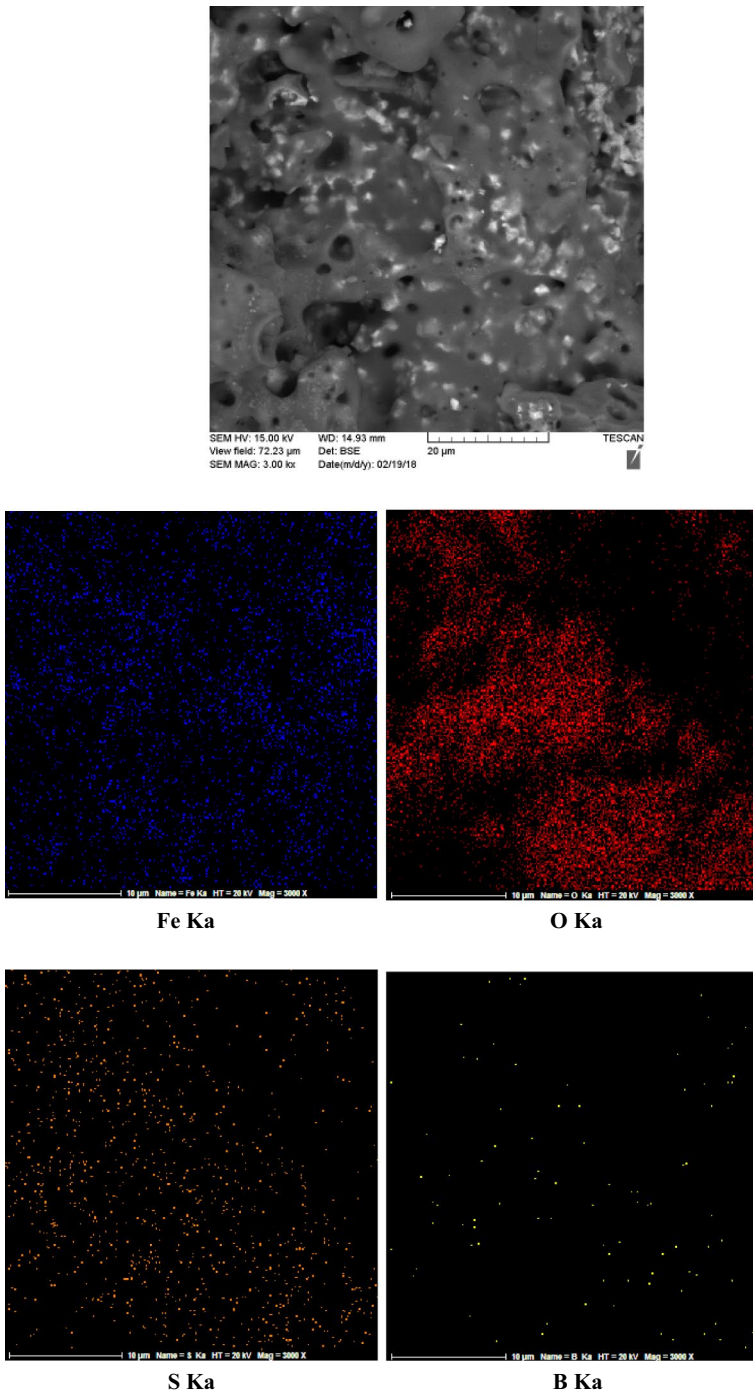


Fig. 9 Mapping analysis of $\text{Fe}_3\text{O}_4@B(\text{HSO}_4)_3$ nanostructures

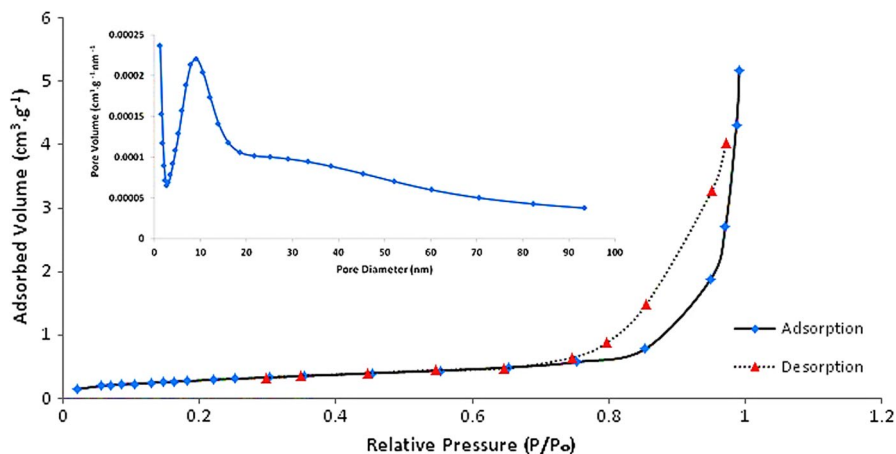


Fig. 10 N₂ adsorption–desorption isotherms (inset) with a corresponding BJH pore-size distribution curve, the pore-size distribution was calculated from the desorption branch of the isotherm

Table 1 Surface data of Fe₃O₄@B(HSO₄)₃

Sample	BET surface area (m ² g ⁻¹)	Pore diameter (cm ³ g ⁻¹)	Pore volume (nm)
SMF/Fe ₃ O ₄ nanospheres	1.055	0.0076	29.143

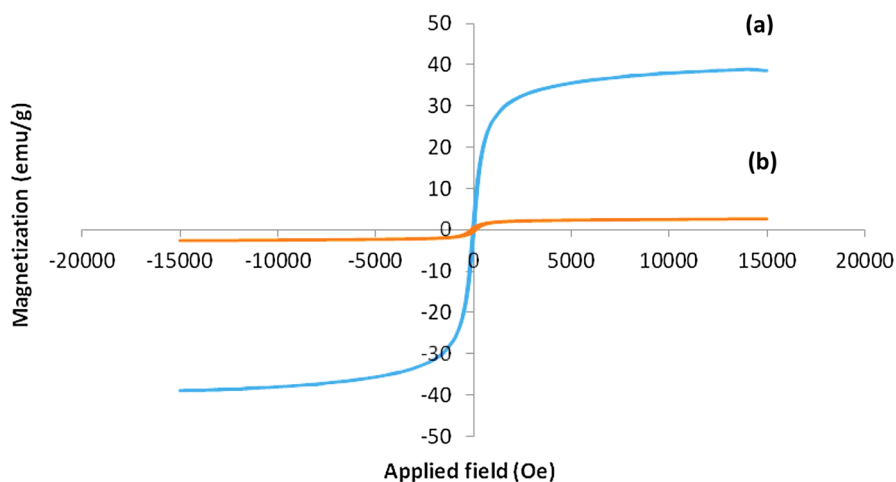
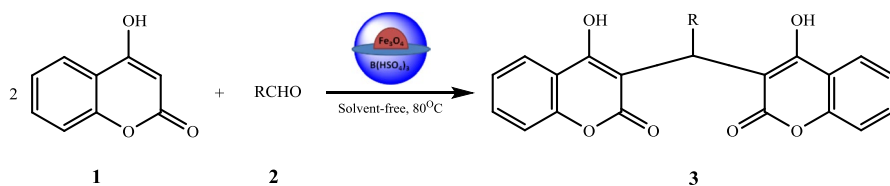


Fig. 11 Magnetization curves for **a** Fe₃O₄, and **b** Fe₃O₄@B(HSO₄)₃

Therefore, it was found that the best reaction conditions for the model reaction were specified to be 1 mmol aldehyde, 2 mmol 4-hydroxycoumarin, and 0.1 g (0.03 wt%) of the Fe₃O₄@B(HSO₄)₃ catalyst under solvent-free conditions at 80 °C as revealed in Table 2.



Scheme 2 Synthesis of biscoumarin derivatives catalyzed by $\text{Fe}_3\text{O}_4 @ \text{B(HSO}_4)_3$

Table 2 Effect of different amounts of $\text{Fe}_3\text{O}_4 @ \text{B(HSO}_4)_3$ and solvents for synthesis of biscoumarin derivatives^a

Entry	Amount of catalyst (wt%)	Condition/solvent	Time (min)	Yield (%) ^a
1	–	80 °C/solvent-free	120	15
2	0.01	80 °C/solvent-free	60	55
3	0.03	80 °C/solvent-free	15	90
4	0.05	80 °C/solvent-free	15	90
5	0.03	r.t./solvent-free	180	15
6	0.03	100 °C/solvent-free	15	92
7	0.03	120 °C/solvent-free	15	95
8	0.03	Reflux/water	60	80
9	0.03	Reflux/ethanol	60	75
10	0.03	Reflux/chloroform	120	55
11	0.03	Reflux/toluene	120	50

Reactions carried out at 10 mmol scale with molar ratio of benzaldehyde:4-hydroxycoumarin:1:2

^aIsolated yield

Table 3 Comparison of one-pot synthesis of biscoumarin **3a** with $\text{Fe}_3\text{O}_4 @ \text{B(HSO}_4)_3$, Fe_3O_4 and $\text{B(HSO}_4)_3$

Entry	Catalyst (0.03 wt%)	Time (min)	Yield (%) ^a
1	$\text{Fe}_3\text{O}_4 @ \text{B(HSO}_4)_3$	15	90
2	Fe_3O_4	20	80
3	$\text{B(HSO}_4)_3$	25	83

Reaction conditions aldehyde (1 mmol); 4-hydroxycoumarin (2 mmol); solvent-free; 80 °C

^aIsolated yield

Catalytic efficiency of the $\text{Fe}_3\text{O}_4 @ \text{B(HSO}_4)_3$, Fe_3O_4 , and $\text{B(HSO}_4)_3$ for the reaction model was evaluated and comparative data are presented in Table 3. It can be seen that $\text{Fe}_3\text{O}_4 @ \text{B(HSO}_4)_3$ was found to be superior in terms of yield and time of reaction. Fe_3O_4 and $\text{B(HSO}_4)_3$ compared to $\text{Fe}_3\text{O}_4 @ \text{B(HSO}_4)_3$ gave slightly lower yields and reaction times were longer. Thus, we can conclude that Fe_3O_4 acts not only as a support, but also it shows good catalytic activity.

The general scope and acceptability of this method have been investigated by the structural variations of simple and readily available aldehydes including

Table 4 Synthesis of biscoumarin derivatives catalyzed by $\text{Fe}_3\text{O}_4@\text{B}(\text{HSO}_4)_3$

Entry	R	Product	Time (min)	Yield (%) ^a	Mp (°C)
1	C_6H_5	3a	15	90	222–224
2	2-HOC ₆ H ₄	3b	15	80	240–242
3	3-NO ₂ C ₆ H ₄	3c	20	85	126–128
4	4-CH ₃ OC ₆ H ₄	3d	10	90	234–236
5	4-HOC ₆ H ₄	3e	15	80	220–222
6	4-NO ₂ C ₆ H ₄	3f	15	85	238–240
7	4-ClC ₆ H ₄	3g	15	80	246–248
8	Ph-CH=CH	3h	30	80	235–237
9	2-Furyl	3i	30	80	194–196
10	CH(CH ₃) ₃	3j	60	–	–

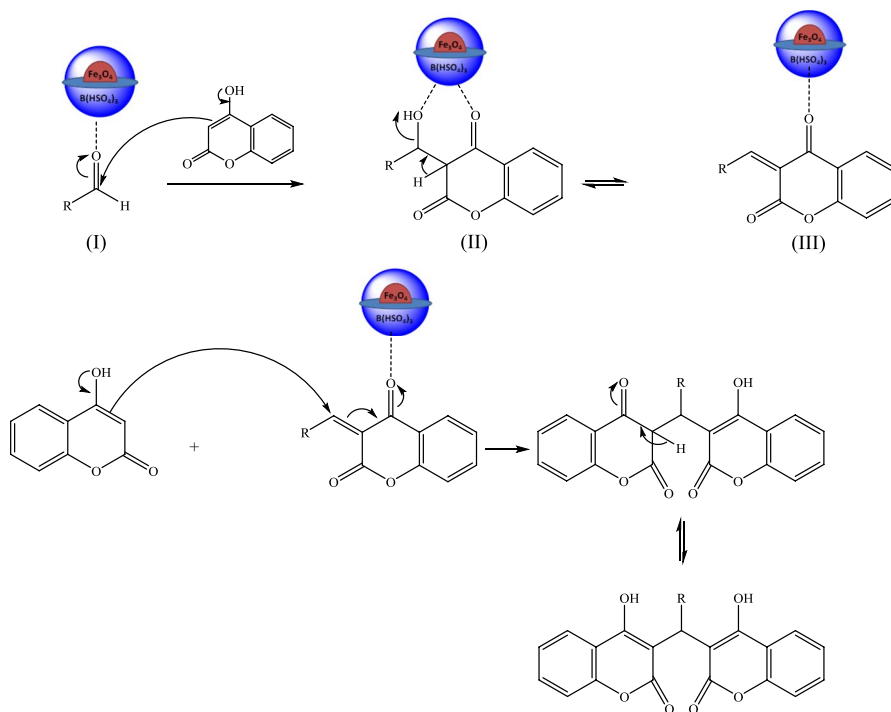
Reaction conditions aldehyde (1 mmol); 4-hydroxycoumarin (2 mmol); $\text{Fe}_3\text{O}_4@\text{B}(\text{HSO}_4)_3$; (0.03 wt%); solvent-free; 80 °C

^aIsolated yields

aromatic, heteroaromatic and aliphatic aldehydes. It has been observed that aldehydes containing OH lead to a faster reaction rate that could be due to the hydrogen bonding of aldehyde with the catalyst (Table 4, entries 2 and 5). The reaction has been performed faster with aldehyde containing OCH₃ group and required less time to give the resulting products (Table 4, entry 4). This catalyst has worked well with aldehydes bearing sensitive functional groups like NO₂, Cl and CH=CH to provide the related products without leading to any side products formation (Table 4, entries 3, 6, 7 and 8). The 2-Furfural as a heteroaromatic aldehyde has been provided as the resultant product with moderate yield (Table 4, entry 9). However, all aromatic aldehydes and heteroaromatic aldehyde have been prepared with the same reactivity and biscoumarin derivatives (entries 1–9, Table 4) but in case of aliphatic aldehydes, reactions have not been done under solvent-free conditions because of low boiling point of the aldehydes (Table 4, entry 10).

The acceptable mechanism for the preparation of biscoumarins using $\text{Fe}_3\text{O}_4@\text{B}(\text{HSO}_4)_3$ is shown in Scheme 3. As regards this, the heterogeneous catalyst acts with both Lewis and Bronsted acid sites, but the main factor of acidity is due to the presence of hydroxyl groups of HSO₄ which is attached to the B atom. In addition, acidity enhancement of catalyst is possible by the activated Lewis acid sites due to a –I effect by attaching HSO₄ to B atoms. According to Banerji's suggestion [41] the acidic nature of a catalyst may simplify carbonyl group activation of aldehyde to give complex **I** and thus an electron-withdrawing carbonyl group can be increased by employing catalyst. The nucleophilic addition of 4-hydroxycoumarin to **I** leads to make **II**. Subsequently, the removal of H₂O from **II** leads to the production of (intermediate) **III** which can be more activated by catalyst. Then, addition of 4-hydroxycoumarin to the activated intermediate **III**, leads to the production of biscoumarin, by the Michael addition method.

Our results were compared to other results which are previously reported for the preparation of biscoumarin derivatives (Table 5).



Scheme 3 Proposed mechanism for the synthesis of biscoumarins catalyzed by $\text{Fe}_3\text{O}_4@\text{B}(\text{HSO}_4)_3$

Furthermore, we evaluated separation and recycling of the $\text{Fe}_3\text{O}_4@\text{B}(\text{HSO}_4)_3$ NPs catalyst which were mentioned in the “[General procedure for recycling of \$\text{Fe}_3\text{O}_4@\text{B}\(\text{HSO}_4\)_3\$ nanoparticles](#)” section. On the basis of the results of reuse of catalyst it was shown that the catalyst can be used four times without significant loss of its catalytic activity (Fig. 12).

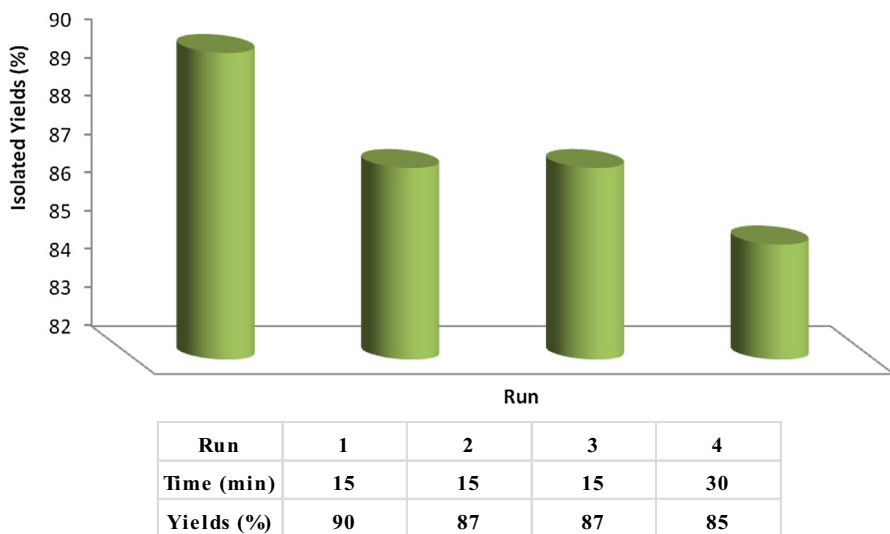
In order to investigate the recycling and reusability of the $\text{Fe}_3\text{O}_4@\text{B}(\text{HSO}_4)_3$, the EDX analysis after four runs showed the presence of sulfur and leaching of sulfur has not occurred (Fig. 13).

Conclusions

In summary, a facile procedure for the synthesis of a $\text{Fe}_3\text{O}_4@\text{B}(\text{HSO}_4)_3$ as a heterogeneous powerful solid acid catalyst which is mediated by solvent-free one-pot synthesis of biscoumarin derivatives is reported in this paper. Tris (hydrogensulfato) boron groups are conveniently loaded on magnetic particles. Magnetic evaluation of $\text{Fe}_3\text{O}_4@\text{B}(\text{HSO}_4)_3$ illustrated the paramagnetic properties of these particles. The separation procedure of this acid magnetic catalyst is performed by the application of an external magnetic source. This method offers considerable advantages including reusability of the catalyst for several times without significant loss in the yield of the reaction, short reaction time, low cost, cleaner reaction profile and ease of

Table 5 Comparison results of $\text{Fe}_3\text{O}_4@\text{B}(\text{HSO}_4)_3$ with some different catalysts reported in the literature in the synthesis of biscoumarin derivatives

Entry	Catalyst	Condition	Time (min)	Yield (%)	References
1	I_2 (10 mol %),	H_2O , reflux	20–32	91–99	[37]
2	[bmim][BF_4] (4 mmol)	Solvent-free, 60–70 °C	120–180	77–91	[38]
3	TBAB (10 mol %)	H_2O , reflux	20–40	77–95	[39]
4	SDS (20 mol %)	H_2O , 60 °C	150–180	78–96	[40]
5	$\text{TiO}_2/\text{SO}_4^{2-}$ (10 mol %)	H_2O , 80 °C	12–30	82–96	[41]
6	[PSebim][OTf] (10 mol %)	Solvent-free, 70 °C	120–180	92–96	[42]
7	[$\text{P}_4\text{VPy-BuSO}_3\text{H}$] HSO_4 (0.1 mmol)	Toluene, 90 °C	36–60	90–95	[43]
8	($\text{H}_{141}\text{[NaP}_5\text{W}_{30}\text{O}_{110}]$)/ SiO_2 (0.3 mol %)	EtOH, r.t	20–40	82–98	[44]
9	Poly(AMPS-co-AA) @ Fe_3O_4 (0.04 mmol)	Toluene, 90 °C	10–33	94–97	[45]
10	CuO-CeO_2 nanocomposite (0.05 g)	H_2O , reflux	8–45	89–94	[46]
11	$\text{B}(\text{HSO}_4)_3$ (0.3 mmol)	EtOH/ H_2O , 70 °C	3–6	81–98	[25]
12	$\text{Fe}_3\text{O}_4@\text{B}(\text{HSO}_4)_3$ (0.03 wt%);	Solvent-free, 80 °C	10–30	70–90	This work

**Fig. 12** Reusability of $\text{Fe}_3\text{O}_4@\text{B}(\text{HSO}_4)_3$ (0.03 wt%); in the reaction of benzaldehyde (1 mmol) with 4-hydroxycoumarin (2 mmol) at 80 °C after 15 min under solvent-free conditions

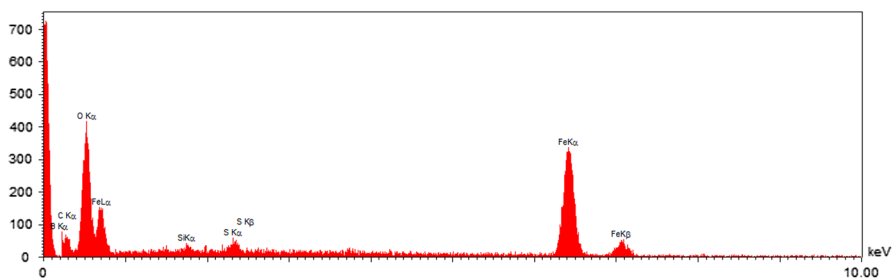


Fig. 13 EDX of $\text{Fe}_3\text{O}_4@\text{B}(\text{HSO}_4)_3$ after 4th run

preparation of catalyst. The main important advantages of this catalyst compared to similar catalysts include smaller particle size, direct connection between tris (hydrogensulfato) boron groups and magnetic particles and finally reduction in the number of catalyst preparation steps.

Acknowledgements The authors acknowledge Firoozabad University Research Council for partial financial support.

References

1. J.A. Melero, R.V. Grieken, G. Morales, *Chem. Rev.* **106**, 3790 (2006)
2. J.A. Melero, J. Iglesias, G. Morales, *Green Chem.* **11**, 1285 (2009)
3. J. Lu, P.H. Toy, *Chem. Rev.* **109**, 815 (2009)
4. S.J. Yuan, X.H. Dai, *Appl. Catal. B Environ.* **154**, 252 (2014)
5. K. Pandey, R.V. Jayaram, M.B. Gawande, R.K. Pandey, R.V. Jayaram, *Catal. Sci. Technol.* **2**, 1113 (2012)
6. M.B. Gawande, P.S. Branco, R.S. Varma, *Chem. Soc. Rev.* **42**, 3371 (2013)
7. M. Fernández-García, J.A. Rodríguez, *Metal Oxide Nanoparticles, Encyclopedia of Inorganic and Bioinorganic, Chemistry* (Wiley, Hoboken, 2011)
8. R.M. Cornell, U. Schwartmann, *The Iron Oxide: Structure, Properties, Reactions, Currences and Uses* (Wiley, Weinheim, 2003)
9. W. Wu, Z. Wu, T. Yu, C. Jiang, W.-S. Kim, *Sci. Technol. Adv. Mater* **16**, 023501 (2015)
10. M.B. Gawande, A. Goswami, T. Asefa, H. Guo, A.V. Biradar, D.-L. Peng, R. Zboril, R.S. Varma, *Chem. Soc. Rev.* **44**, 7431 (2015)
11. A. Hu, G.T. Yee, W. Lin, *J. Am. Chem. Soc.* **127**, 12486 (2005)
12. A. Schätz, M. Hager, O. Reiser, *Adv. Funct. Mater.* **19**, 2109 (2009)
13. M.A. Ghasemzadeh, J. Safaei-Ghomi, S. Zahedi, *J. Serb. Chem. Soc.* **78**, 769 (2013)
14. K. Karami, S. Dehghani Najvani, N. Haghghat Naeini, P. Hervés, *Chin. J. Catal.* **36**, 1047 (2015)
15. M.A. Ghasemzadeh, *Acta Chim. Slov.* **62**, 977 (2015)
16. M.A. Ghasemzadeh, *Quim. Nova* **1**, 47 (2017)
17. R.B. Kistler, C. Helvac, Boron and borates, in *Industrial minerals and rocks*, 6th edn., ed. by D.D. Carr (SME, Littleton, 1994), p. 171
18. I. Tsuyumoto, T. Oshio, *J. Wood Chem. Technol.* **29**, 277 (2009)
19. Method 3052 microwave assisted acid digestion of siliceous and organically based matrices (PDF) US EPA 2015-06-22
20. J. Dempsey (2009) [1998] "BORAX" dempsey's forge retrieved 2010-07-23 (2009)
21. F. Prager, Science becomes a toy-silly putty. loti.com. Rewind the fifites. Retrieved 06 July 2013
22. A.R. Kiasat, M. Fallah-Mehrjardi, *J. Braz. Chem. Soc.* **19**, 1595 (2008)
23. Z. Karimi-Jaberi, B. Pooladian, *Monatshefte für Chemie.* **144**, 659 (2013)
24. Z. Karimi-Jaberi, A. Jaafarzadeh, *Res. Chem. Intermed.* **41**, 4913 (2015)

25. Z. Karimi-Jaberi, M.R. Nazarifar, B. Pooladian, *Chin. Chem. Lett.* **23**, 781 (2012)
26. M. Soheilzad, M. Adib, S. Sajjadifar, *Monatshefte für Chemie* **144**, 1353 (2014)
27. H.R. Safaei, M. Davoodi, M. Shekouhy, *Synth. Commun.* **43**, 2178 (2013)
28. S.J. Saghanezhad, H.R. Safaei, *J. Serb. Chem. Soc.* **78**, 1481 (2013)
29. A. Khalafi-Nezhad, H. Foroughi, M.M. Doroodmand, F. Panahi, *J. Mater. Chem.* **21**, 12842 (2011)
30. M. Farahi, B. Karami, R. Keshavarz, F. Khosravian, *RSC Adv.* **7**, 46644 (2017)
31. A. Maresca, A. Scozzafava, C.T. Supuran, *Bioorg. Med. Chem. Lett.* **20**, 7255 (2010)
32. N. Vukovic, S. Sukdolak, S. Solujic, N. Niciforovic, *Food Chem.* **120**, 1011 (2010)
33. F. Carta, A. Maresca, A. Scozzafava, C.T. Supuran, *Bioorg. Med. Chem.* **20**, 2266 (2012)
34. R. Okenne, R.D. Thomes, *Coumarins: Biology, Application, and Modes of Action* (Wiley, Chichester, 1997)
35. M. Zahradnik, *The Production and Application of Fluorescent Brightening Agents* (Wiley, Chichester, 1992)
36. C. Ranjitha, K.K. Vijayan, V.K. Praveen, N.S. Saleesh Kumar, *Spectrochim Acta A* **75**, 1610 (2010)
37. M. Kidwai, V. Bansal, P. Mothsra, S. Saxena, R.K. Somvanshi, S. Dey, T.P. Singh, *J. Mol. Catal. A: Chem.* **268**, 76 (2007)
38. J.M. Khurana, S. Kumar, *Monatsh. Chem.* **141**, 561 (2010)
39. J.M. Khurana, S. Kumar, *Tetrahedron Lett.* **50**, 4125 (2009)
40. H. Mehrabi, H. Abusaidi, *J. Iran. Chem. Soc.* **7**, 890 (2010)
41. B. Karmakar, A. Nayak, J. Banerji, *Tetrahedron Lett.* **53**, 4343 (2012)
42. W. Li, Y. Wang, Z. Wang, L. Dai, Y. Wang, *Catal. Lett.* **141**, 1651 (2011)
43. K. Parvanak Boroujeni, P. Ghasemi, Z. Rafienia, *Monatsh Chem.* **145**, 1651 (2014)
44. M.M. Heravi, F. Nahavandi, S. Sadjadi, H.A. Oskooie, F.F. Bamoharram, *Synth. Commun.* **145**, 498 (2010)
45. K. Parvanak Boroujeni, S. Hadizadeh, S. Hasani, A. Fadavi, M. Shahrokh, *Acta Chim. Slov.* **64**, 692 (2017)
46. J. Albadi, A. Mansournezhad, S. Salehnasab, *Res. Chem. Intermed.* **41**, 5713 (2015)
47. S. Rahmani, B. Zeynizadeh, *Res. Chem. Intermed.* **45**, 1227 (2019)
48. R. Rezaei, F. Moezzi, M.M. Doroodmand, *Chin. Chem. Lett.* **25**, 183 (2014)
49. R. Rezaei, M.R. Sheikhi, *Res. Chem. Intermed.* **41**, 1283 (2015)
50. F. Gholamian, M. Shabanian, M. Shahrokh, *J. Clust. Sci.* **24**, 177 (2013)
51. L. Boroica, D. Radu, R. Medianu, *J. Optoelectron. & Adv. Mater.* **10**, 3217 (2008)
52. A. Alinasab Amiri, S. Javanshir, Z. Dolatkah, M.G. Dekamin, *New J. Chem.* **39**, 9665 (2015)
53. M.A. Ghasemzadeh, J. Safaei-Ghomi, H. Molaei, *C. R. Chimie.* **15**, 969 (2012)
54. S.H. Dewi, W.A. Adi, *J. Phys. Conf. Ser.* **1091**, 012021 (2018)
55. A. Ruiz-Baltazar, R. Esparza, G. Rosas, R. Pérez, *J Nanomater.* **16**, 1 (2015)
56. E. Moroydor Derun, P. Gurses, M. Yildirim, A.S. Kipcak, T. Ibroska, S. Piskin, *Int. Sch. Sci. Res. Innov.* **8**, 565 (2014)
57. M.B. Gawande, A.K. Rathi, I.D. Nogueira, R.S. Varma, P.S. Branco, *Green Chem.* **15**, 1895 (2013)
58. F. Sevim, F. Demir, M. Bilen, H. Okur, *Korean J. Chem. Eng.* **23**, 736 (2006)
59. K. Onar, M.E. Yakinci, *Journal of Physics: 9th International Conference on Magnetic and Superconducting Materials (MSM15)* 667, Antalya, Turkey, 30 April to 3 May 2015
60. S. Brunauer, L.S. Deming, W.E. Deming, E. Teller, *J. Am. Chem. Soc.* **62**, 1723 (1940)
61. G. Leofanti, M. Padovan, G. Tozzola, B. Venturelli, *Catal. Today* **41**, 207 (1998)